J Periodontal Implant Sci. 2023 Feb;53(1):20-37
https://doi.org/10.5051/jpis.2105700285
pISSN 2093-2278·eISSN 2093-2286

JPIS
Journal of Periodontal & Implant Science

Research Article
Periodontal Science

Check for updates

Sequential anti-inflammatory and osteogenic effects of a dual drug delivery scaffold loaded with parthenolide and naringin in periodontitis

Rui Chen [1,2], **Mengting Wang** [1,2], **Qiaoling Qi** [3], **Yanli Tang** [1,2], **Zhenzhao Guo** [4], **Shuai Wu** [4], **Qiyan Li** [1,2,*]

[1]Department of Stomatology, The First People's Hospital of Yunnan Province, Kunming, China
[2]The Affiliated Hospital of Kunming University of Science and Technology, Kunming, China
[3]Yunnan Provincial Key Laboratory of Entomological Biopharmaceutical R&D, Dali University, Dali, China
[4]Jinan University, Guangzhou, China

OPEN ACCESS

Received: Nov 5, 2021
Revised: May 28, 2022
Accepted: Jun 6, 2022
Published online: Jul 25, 2022

***Correspondence:**
Qiyan Li
Department of Stomatology, The First People's Hospital of Yunnan Province, No. 157 Jinbi Street, Kunming, Yunnan 650032, China.
Email: ynliqiyan@aliyun.com
Tel: +86-15368088803
Fax: +86-087163638218

ORCID iDs
Rui Chen
https://orcid.org/0000-0003-3396-7827
Mengting Wang
https://orcid.org/0000-0002-9009-5386
Qiaoling Qi
https://orcid.org/0000-0001-5880-3170
Yanli Tang
https://orcid.org/0000-0001-8119-3024
Zhenzhao Guo
https://orcid.org/0000-0003-4262-130X
Shuai Wu
https://orcid.org/0000-0003-4343-5103
Qiyan Li
https://orcid.org/0000-0002-5558-2330

ABSTRACT

Purpose: Our pilot study showed that a 3-dimensional dual drug delivery scaffold (DDDS) loaded with Chinese herbs significantly increased the regenerated bone volume fraction. This study aimed to confirm the synergistic anti-inflammatory and osteogenic preclinical effects of this system.
Methods: The targets and pathways of parthenolide and naringin were predicted. Three cell models were used to assess the anti-inflammatory effects of parthenolide and the osteogenic effects of naringin. First, the distance between the cementoenamel junction and alveolar bone crest (CEJ-ABC) and the bone mineral density (BMD) of surgical defects were measured in a rat model of periodontitis with periodontal fenestration defects. Additionally, the mRNA expression levels of matrix metallopeptidase 9 (MMP9) and alkaline phosphatase (ALP) were measured. Furthermore, the number of inflammatory cells and osteoclasts, as well as the protein expression levels of tumor necrosis factor-alpha (TNF-α) and levels of ALP were determined.
Results: Target prediction suggested prostaglandin peroxidase synthase (PTGS2) as a potential target of parthenolide, while cytochrome P450 family 19 subfamily A1 (CYP19A1) and taste 2 receptor member 31 (TAS2R31) were potential targets of naringin. Parthenolide mainly targeted inflammation-related pathways, while naringin participated in steroid hormone synthesis and taste transduction. *In vitro* experiments revealed significant anti-inflammatory effects of parthenolide on RAW264.7 cells, and significant osteogenic effects of naringin on bone marrow mesenchymal stem cells and MC3T3-E1 cells. DDDS loaded with parthenolide and naringin decreased the CEJ-ABC distance and increased BMD and ALP levels in a time-dependent manner. Inflammation was significantly alleviated after 14 days of DDDS treatment. Additionally, after 56 days, the DDDS group exhibited the highest BMD and ALP levels.
Conclusions: DDDS loaded with parthenolide and naringin in a rat model achieved significant synergistic anti-inflammatory and osteogenic effects, providing powerful preclinical evidence.

Keywords: Drug delivery systems; Naringin; Parthenolide; Periodontitis

Conflict of Interest
No potential conflict of interest relevant to this article was reported.

Author Contributions
Conceptualization: Zhenzhao Guo, Qiyan Li; Formal analysis: Rui Chen, Mengting Wang, Qiaoling Qi; Investigation: Mengting Wang, Shuai Wu; Methodology: Yanli Tang, Shuai Wu; Project administration: Yanli Tang, Qiyan Li; Writing - original draft: Rui Chen, Mengting Wang, Qiaoling Qi; Writing - review & editing: Zhenzhao Guo, Qiyan Li.

INTRODUCTION

Periodontitis is 1 of the 2 most common oral diseases. It is a chronic inflammatory disease that leads to tooth loss and irreversible alveolar bone resorption [1]. Clinically, local administration of medication is often used to control inflammation. The drugs used are mostly antibacterial agents, such as nitroimidazole, tetracycline, and macrolide antibiotics [2]. Although guided tissue regeneration (GTR) promotes periodontal membrane reattachment and epithelial reconstruction [3], conventional GTR promotes neither the differentiation and maturation of osteoblasts nor the regeneration of alveolar bone. A controlled-release drug delivery system can prolong the time that drugs remain in the affected area, segment the administration of medications, and facilitate a timed, quantitative, and uniformly targeted treatment [4]. For example, bone morphogenetic protein-2 (BMP-2) hydrogels with chitosan (CS) have been found to induce new alveolar bone formation, promote jaw healing, and guide periodontal tissue regeneration [5].

Our pilot study established a robust 3-dimensional (3D) DDDS loaded with traditional Chinese herbs (parthenolide and naringin) to regenerate periodontal tissue and control inflammation. This system has shown excellent biocompatibility and biodegradability, and it achieved the desired hierarchical release profiles [6]. Parthenolide (C15H20O3; MR248.3) is isolated from feverfew (*Tanacetum parthenium*) and exhibits substantial anti-tumor, anti-inflammatory, and anti-allergenic effects [7]. By inhibiting the expression of tumor necrosis factor (TNF)-α, interleukin (IL)-1 beta, IL-6, and nitric oxide synthase 2 (NOS2), parthenolide exerts significant anti-inflammatory effects through the nuclear factor (NF)-kappa B pathway [8]. Naringin (C27H32O14; MR580.53) is the main pharmacodynamic component of the Chinese folk prescription *Drynaria fortunei* J. Sm. (Kunze), which has been reported to repair alveolar bone defects [9]. Additionally, naringin is thought to increase the ratio of osteoprotegerin (OPG) to receptor activator of NF-κB ligand (RANKL) by increasing the mRNA expression of OPG and decreasing the mRNA expression of RANKL, thereby achieving osteogenesis [10].

In this study, we further hypothesized that the poly-L-lactic acid (PLLA)/CS controlled release system loaded with parthenolide and naringin would exert an excellent multistage therapeutic effect in a rat model of periodontitis with periodontal fenestration defects; specifically, inflammation would first be controlled, and bone tissue would then be regenerated. A bioinformatics analysis was first conducted to predict the targets and pathways of parthenolide and naringin. Three cell models were used to assess the anti-inflammatory effects of parthenolide and the osteogenic effects of naringin. Finally, a rat model of periodontitis with periodontal fenestration defects was established to investigate the compound therapeutic effect of the PLLA/CS controlled release system loaded with parthenolide and naringin. This study provides preclinical evidence that DDDS loaded with parthenolide and naringin can be used to treat periodontal disease.

MATERIALS AND METHODS

Target and pathway prediction

The Simplified Molecular-Input Line Entry System (SMILES) formulas of parthenolide and naringin were searched in the DrugBank database with the query ID DB13063 and CID 442428, respectively (https://go.drugbank.com/drugs/). HitPickV2, the similarity ensemble

https://doi.org/10.5051/jpis.2105700285

approach (SEA) algorithm, and the Swiss Target Prediction database were used to predict the potential targets of parthenolide and naringin [11-13]. Targets with $P<0.05$, Tanimoto coefficient=1, or predicted precision >0.5 were identified as potential targets, and the prediction results were displayed using a Venn diagram.

Based on the common targets predicted above, the Gene MANIA prediction server (http://www.genemania.org/), the STRING web server (https://string-db.org/cgi/input.pl), and the HumanBase web server (https://hb.flatironinstitute.org/) were used to perform functional interaction, protein-protein interaction (PPI) and tissue-specific gene network analyses, respectively [14-16]. The enriched biological functions and interactions were automatically generated by these servers.

Cell models

Anti-inflammatory effect of parthenolide on RAW264.7 cells

RAW264.7 cells were purchased from the Kunming Institute of Zoology, Chinese Academy of Sciences and cultured in DMEM (HyClone, Logan, UT, USA). Dimethyl sulfoxide (DMSO), 10 μM parthenolide (Promega, Madison, WI, USA), and 10 μM BAY 11-7082 (NF-κB inhibitor; Cell Signaling Technology, Danvers, MA, USA) were added to the media in culture plates (n=3); 1 hour later, 100 ng/mL *Escherichia coli* lipopolysaccharide (LPS; Sigma, St. Louis, MO, USA) was added to all groups. After culturing for 4 and 8 hours, the total RNA was extracted using an Eastep Super total RNA extraction kit (LS1040, Promega, Madison, WI, USA). The mRNA expression levels of IL-1β, IL-6, TNF-α, IL-10, matrix metallopeptidase (MMP) 13, NOS2, and PTGS2 were detected by quantitative reverse transcription-polymerase chain reaction (qRT-PCR). After culturing for 24 and 48 hours, the supernatant of the cells was collected to assess the expression of IL-6 and TNF-α by enzyme-linked immunosorbent assay (ELISA; M&P, Brooksville, FL, USA). After 15, 30, and 60 minutes of culture in the plates, total protein was extracted using a DC Protein Assay kit (Bio-Rad, Hercules, CA, USA), and the expression levels of phospho-p65, phospho-p38, phospho-ERK, and phospho-JNK were detected by western blotting (Cell Signaling Technology).

The membrane addition experiment was divided into 3 groups: DMSO, a blank polylactide-coglycolide (PLGA)/PLLA composite fiber membrane (P/P), and a PLGA/PLLA membrane loaded with parthenolide (PTL + P/P, fabricated by electrostatic spinning). After culture for 7 days, *E. coli* LPS (100 ng/mL) was added, and the same procedures were performed to detect all the molecular markers mentioned above.

Osteogenic effect of naringin

Mouse bone marrow mesenchymal stem cells (BMSCs) were obtained from 1-month-old BALB/c and Kunming mice purchased from Kunming Ainimo Experimental Animal Co., Ltd. (Kunming, China). The differentiation of BMSCs requires osteogenic induction solution, which comprises 10 mmol/L β-sodium glycerophosphate (Sigma), 50 mg/L vitamin C and 0.1 μmol/L dexamethasone (Meilunbio, Dalian, China). MC3T3-E1 cells were purchased from Kunming Cell Bank, Chinese Academy of Sciences. After culture in α-MEM (HyClone, Logan, UT, USA), the cells were transferred to 12-well plates, cultured for 12 hours, starved for 12 hours, and then treated with 10 μL of DMSO (10 μM), 1 μM, or 0.1 μM naringin (Sigma) and 100 ng/mL recombinant human bone morphogenetic protein-2 (rhBMP2, Peprotech, Cranbury, NJ, USA). The samples were collected at different time points. The mRNA expression of ALP, collagen I (ColI), osteocalcin (OC), OPG, osteopontin (OPN), and runt-related transcription factor 2 (RUNX2) in BMSCs and MC3T3-E1 cells were detected by qRT-

https://doi.org/10.5051/jpis.2105700285

PCR. ALP activity was detected with an ALP Assay Kit (P0321S; Beyotime, Shanghai, China), and the concentration of the osteogenic protein OC was detected by ELISA (CSB-E17681m; Cusabio, Wuhan, China).

Rat model

The medical ethics committee approved all the experimental procedures at Dali University, Yunnan Province, China (approval No. AEWC-2019-PZ-15).

Male Sprague-Dawley rats (230–250 g, n=130; Hunan Slack Experimental Animal Co., Ltd., Hunan, China) were given free access to food pellets and water in an air-conditioned environment (22°C, 50% humidity, natural light from 07:00 to 19:00). Individual rats were randomly divided into the healthy, model, scaffold (implantation of blank PLLA/CS scaffold), DDDS (PLLA/CS controlled release system loaded with parthenolide and naringin), and GBOC (implantation of Geistlich Bio-OSS® Collagen II; Geistlich, Wolhusen, Switzerland) groups. After anesthetization with 10% chloral hydrate, the right mandibular first molars of the rats (except the healthy group) were ligated using 2-0 silk thread (**Supplementary Figure 1A**). One week later, periodontal fenestration defects measuring 3 mm × 2 mm × 1 mm were created (**Supplementary Figure 1B**) [17]. Six right mandibular bones in the model group were analyzed by scanning electron microscopy (SEM) to assess whether the model was successfully established. The rats were sacrificed by cervical dislocation 14, 28, and 56 days after administration. The gingival tissue around the first and second molars was removed by a surgical procedure and stored in liquid nitrogen immediately. The mandibles were collected and fixed in formalin for 48 hours at 4°C, followed by transfer to 70% ethanol for micro-computed tomography (CT) scanning (XTV160H, X-TEK, LITH, IL, UK). After micro-CT, specimens were embedded in paraffin and serially sectioned (3-μm). Mimics 17.0 (Materialise, Leuven, Belgium) was used for the 3D reconstruction of defects, and to determine the distance between the cementoenamel junction and alveolar bone crest (CEJ-ABC) and the bone mineral density (BMD) of each sample [18,19]. In short, for each sample, the bone density of 130 layers beneath the cementum-enamel boundary plane was measured with fixed length and width parameters. The BMD of each sample was then determined by calculating the mean value of bone density across all 130 layers. The mRNA expression of IL-6, IL-1β, MMP-2, MMP-9, ALP, OPG, and RANKL in periodontal tissues was detected using quantitative reverse transcription polymerase chain reaction (qRT-PCR). The number of inflammatory cells and the region size of defects were detected by hematoxylin-eosin staining. The size of defects was measured using the following method: The length of the defect was determined by multiplying the number of sections in which defects were seen by the thickness of each section (3 μm). The width and depth of the defect was approximated by calculating the mean value of each measurement across the sections with the largest defect and the first and last sections. The number of osteoclasts was detected by tartrate-resistant acid phosphatase staining. Immunohistochemical (IHC) staining was used to measure the expression of TNF-α and ALP.

Statistical analysis

Bioinformatics analyses were conducted using R v3.6.1. All the experimental data are expressed as the mean ± standard error, and 1-way analysis of variance (ANOVA) was performed with the Tukey or Games-Howell post hoc test (SPSS 22.0; IBM Corp., Armonk, NY, USA). *P* values <0.05 were considered statistically significant.

https://doi.org/10.5051/jpis.2105700285

RESULTS

Target and pathway prediction

The SMILES formulas of parthenolide and naringin were C\\C1=C/CC[C@@]2(C)O[C@H]2[C@H]2OC(=O)C(=C)[C@@H] and CC1C(C(C(C(O1)OC2C(C(C(OC2OC3=CC(=C4C(=O)CC(OC4=C3)C5=CC=C(C=C5)O)O)CO)O)O)O)O)O)O, respectively (**Figure 1A**). The target prediction results suggested that prostaglandin peroxidase synthase (PTGS2) was a potential target of parthenolide, while cytochrome P450 family 19 subfamily A1 (CYP19A1) and taste 2 receptor member 31 (TAS2R31) were potential targets of naringin (**Figure 1B**).

Three network analyses of these target genes were performed. Gene MANIA network analysis (**Figure 1C**, **Table 1**) showed that the target genes of parthenolide were mainly involved in oxidoreductase peroxidase and antioxidant-related processes, while the target genes of naringin especially participated in transcription, response to nutrients, taste and xenobiotic stimulus processing.

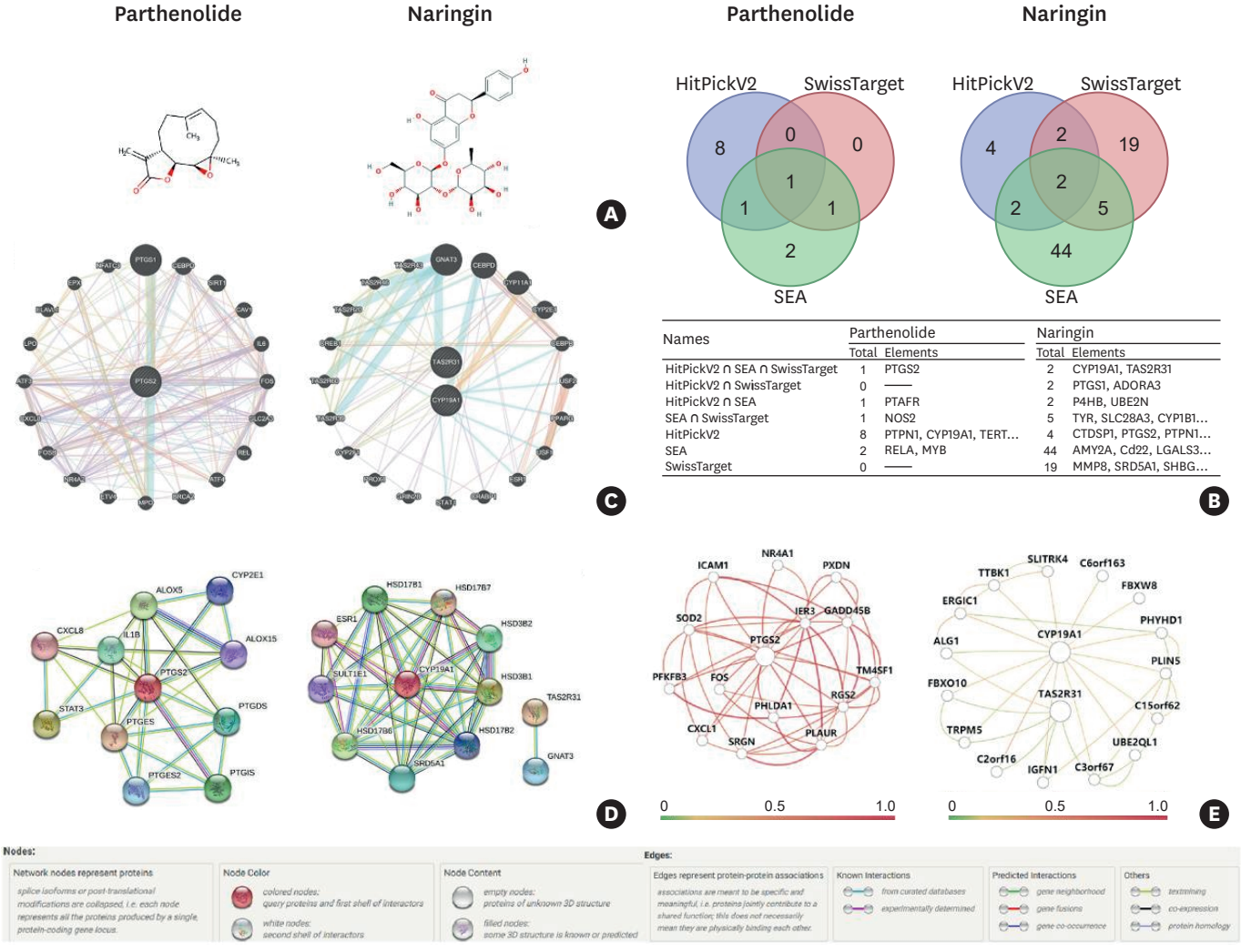

Names	Parthenolide		Naringin	
	Total	Elements	Total	Elements
HitPickV2 ∩ SEA ∩ SwissTarget	1	PTGS2	2	CYP19A1, TAS2R31
HitPickV2 ∩ SwissTarget	0	——	2	PTGS1, ADORA3
HitPickV2 ∩ SEA	1	PTAFR	2	P4HB, UBE2N
SEA ∩ SwissTarget	1	NOS2	5	TYR, SLC28A3, CYP1B1…
HitPickV2	8	PTPN1, CYP19A1, TERT…	4	CTDSP1, PTGS2, PTPN1…
SEA	2	RELA, MYB	44	AMY2A, Cd22, LGALS3…
SwissTarget	0	——	19	MMP8, SRD5A1, SHBG…

Figure 1. Target and pathway prediction. (A) Molecular structures of parthenolide and naringin, and (B) their target predictions, (C) gene functional interaction by GeneMANIA, (D) protein-protein interaction by STRING, and (E) tissue-specific network analyses by HumanBase.

https://doi.org/10.5051/jpis.2105700285

Table 1. GeneMANIA network function enrichment of parthenolide and naringin

Function	Parthenolide	Naringin
Oxidoreductase activity, acting on peroxide as acceptor	3.38E-04	
Peroxidase activity	3.38E-04	
Antioxidant activity	1.95E-03	
Cellular response to reactive oxygen species	1.96E-03	
Response to oxidative stress	2.16E-03	
Prostaglandin biosynthetic process	2.33E-03	
Prostanoid biosynthetic process	2.33E-03	
Response to reactive oxygen species	2.33E-03	
Regulation of nuclease activity	2.33E-03	
Prostaglandin metabolic process	3.31E-03	
Prostanoid metabolic process	3.31E-03	
Cellular response to oxidative stress	4.77E-03	
Cellular response to hydrogen peroxide	1.03E-02	
Icosanoid biosynthetic process	1.05E-02	
Fatty acid derivative biosynthetic process	1.05E-02	
Inflammatory response	1.14E-02	
Positive regulation of response to external stimulus	1.14E-02	
Response to hydrogen peroxide	1.14E-02	
Unsaturated fatty acid biosynthetic process	1.32E-02	
Regulation of fatty acid metabolic process	1.80E-02	
Sequence-specific DNA binding RNA polymerase II transcription factor activity		5.71E-07
RNA polymerase II distal enhancer sequence-specific DNA binding transcription factor activity		9.20E-05
Sequence-specific DNA binding		1.88E-03
Monooxygenase activity		3.34E-03
Sensory perception of bitter taste		3.89E-03
Oxidoreductase activity, acting on paired donors, with incorporation or reduction of molecular oxygen		7.09E-03
Positive regulation of fat cell differentiation		7.80E-03
Regulatory region DNA binding		1.65E-02
Sensory perception of taste		1.65E-02
Regulatory region nucleic acid binding		1.65E-02
Transcription regulatory region DNA binding		1.65E-02
Response to nutrient		1.65E-02
Cellular response to xenobiotic stimulus		2.73E-02
Response to xenobiotic stimulus		2.73E-02
Xenobiotic metabolic process		2.73E-02
Heme binding		2.73E-02
Regulation of fat cell differentiation		3.02E-02
Tetrapyrrole binding		3.02E-02

Each line indicates the pathway and *P* value of naringenin and estrone.

Protein-protein interaction network analysis (**Figure 1D**, **Supplementary Table 1**) suggested that parthenolide-related genes were mainly involved in fatty acid biosynthetic and metabolic processes (such as cyclooxygenase and lipoxygenase) and inflammatory responses, particularly cytokine pathways. However, naringin-related genes were involved in hormone and steroid biosynthetic, metabolic, and catabolic processes (particularly sex hormones) and sexual organ development pathways. Furthermore, the KEGG enriched pathways (**Supplementary Table 2**) indicated that ovarian steroidogenesis was the only common pathway affected by parthenolide and naringin. Thus, parthenolide mainly targets inflammation-related diseases and pathways, while naringin participates in steroid hormone synthesis and taste transduction.

Tissue-specific network analysis (**Figure 1E**) revealed the target genes of parthenolide and naringin. However, the tissue-specific network analysis found no significant gene enrichment related to either drug.

https://doi.org/10.5051/jpis.2105700285

Anti-inflammatory effects of parthenolide and osteogenesis effects of naringin in cell models

Compared with DMSO-treated cells, parthenolide-treated RAW264.7 cells exhibited significantly lower mRNA expression of IL-1β, IL-6, TNF-α, MMP13, NOS2, and PTGS2 after 4 and 8 hours of LPS stimulation (P<0.001; **Figure 2A**). The mRNA expression of IL-1β, NOS2, and PTGS2 significantly decreased in the parthenolide + P/P group at 8 hours (P<0.001; **Supplementary Figure 2A**). The mRNA expression of IL-10 significantly decreased only in the parthenolide group at 4 hours (P<0.01), while in the parthenolide + P/P group, it showed a non-significant tendency to decrease (P>0.05; **Supplementary Figure 2B**). The expression levels of IL-6 (24 and 48 hours) and TNF-α (24 hours) also significantly decreased in the parthenolide and BAY group (P<0.01; **Figure 2C**). The protein expression of phospho-p65 and phospho-JNK in the parthenolide group significantly decreased compared with that in the DMSO group at 15 minutes (**Figure 2F**); however, the phospho-p65 protein was retained at low levels in the parthenolide + P/P group throughout the testing period (**Supplementary Figure 2D**). The expression of phospho-p38 in the parthenolide + P/P group significantly increased compared with that in the DMSO group at 15 and 60 minutes (P<0.01; **Supplementary Figure 2E**), The expression of phospho-ERK showed no differences in either the parthenolide or parthenolide + P/P group (P>0.05; **Supplementary Figure 2E**).

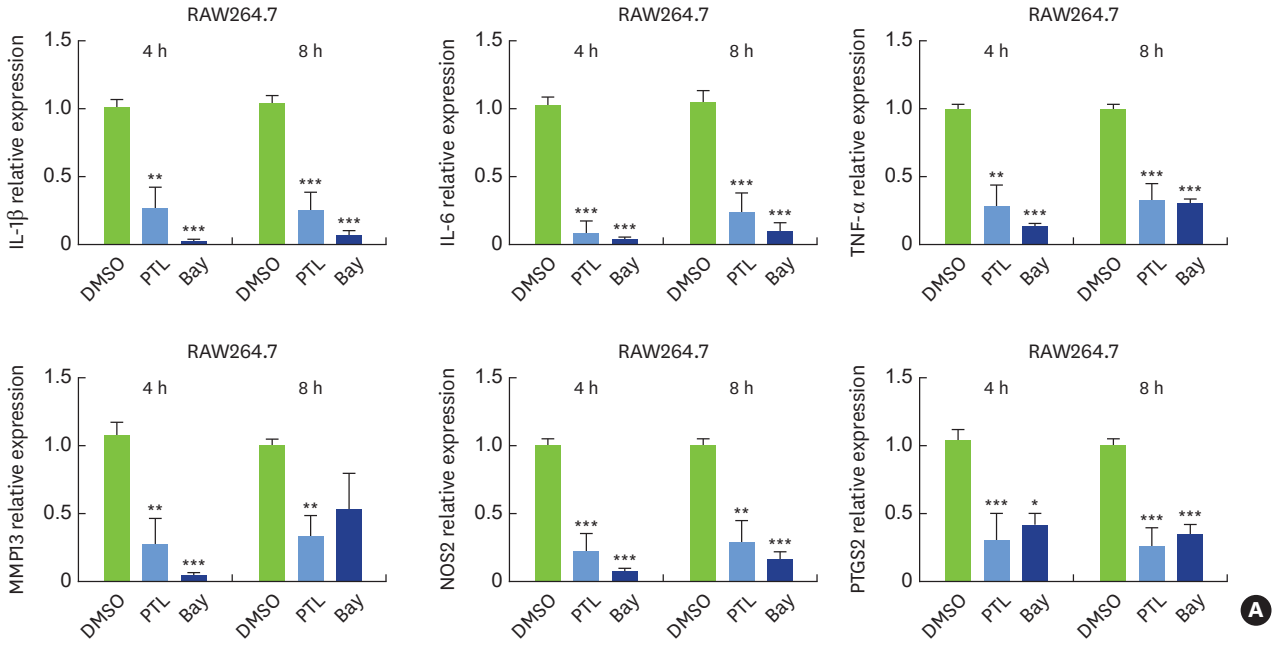

Figure 2. Cell models. (A) the effect of PTL on the mRNA expression of IL-1β, IL-6, TNF-α, MMP13, NOS2 and PTGS2 in RAW264.7 cell; (B) the effect of NG on the mRNA expression of OC and OPG in BMSC and ColI in MC3T3-E1 cells; (C) the effect of PTL on the expression of IL-6 and TNF-α in RAW264.7 cell; (D) the effects of NG on the ALP activity of MC3T3-E1 cell; (E) the effects of NG on the concentration of OC in BMSC cell; (F) the effect of PTL on the protein expression of phospho-p65 and phospho-JNK in RAW264.7 cell.
Values are means ± standard error, n=9.
PTL: parthenolide, IL: interleukin, TNF: tumor necrosis factor, MMP: matrix metallopeptidase, NOS: nitric oxide synthase, PTGS2: prostaglandin peroxidase synthase, NG: naringin, OC: osteocalcin, OPG: osteoprotegerin, BMSC: bone marrow mesenchymal stem cell, ColI: collagen I, ALP: alkaline phosphatase, DMSO: dimethyl sulfoxide, ANOVA: analysis of variance.
$^{*}P$<0.05, $^{**}P$<0.01, $^{***}P$<0.001 vs. DMSO; as evaluated by one-way ANOVA followed by Tukey's test for multiple comparisons. (PTL represented group of 10 μM parthenolide, Bay represented 10 μM Bay 11-7082 (NF-κB inhibitor), NG 10 μM, 1 μM or 0.1 μM represented naringin at 10 μM, 1 μM or 0.1 μM, and rhBMP2 represented 100 ng/mL recombinant human bone morphogenetic protein-2, respectively.

(continued to the next page)

https://doi.org/10.5051/jpis.2105700285

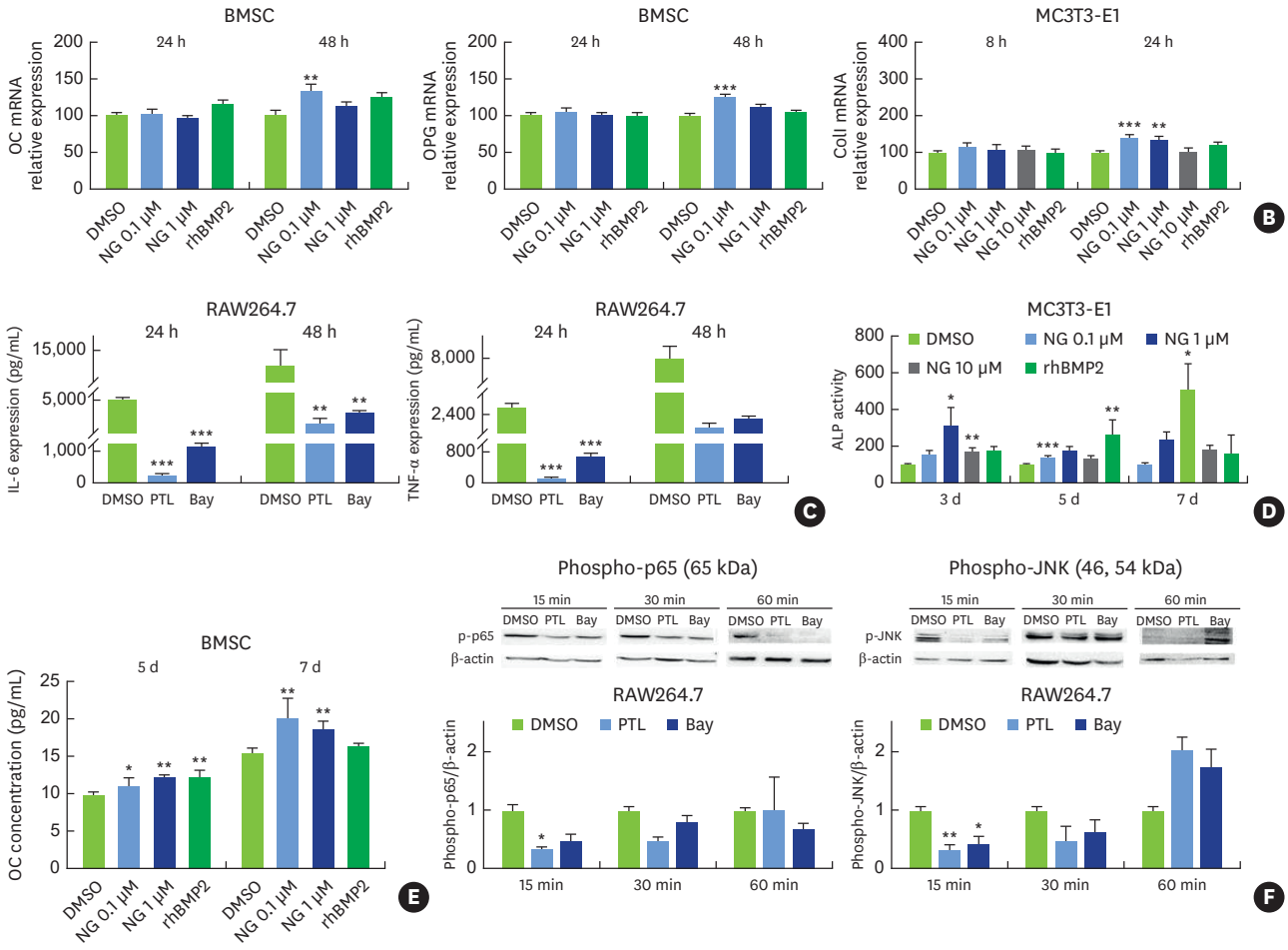

Figure 2. (Continued) Cell models. (A) the effect of PTL on the mRNA expression of IL-1β, IL-6, TNF-α, MMP13, NOS2 and PTGS2 in RAW264.7 cell; (B) the effect of NG on the mRNA expression of OC and OPG in BMSC and ColI in MC3T3-E1 cells; (C) the effect of PTL on the expression of IL-6 and TNF-α in RAW264.7 cell; (D) the effects of NG on the ALP activity of MC3T3-E1 cell; (E) the effects of NG on the concentration of OC in BMSC cell; (F) the effect of PTL on the protein expression of phospho-p65 and phospho-JNK in RAW264.7 cell.
Values are means ± standard error, n=9.
PTL: parthenolide, IL: interleukin, TNF: tumor necrosis factor, MMP: matrix metallopeptidase, NOS: nitric oxide synthase, PTGS2: prostaglandin peroxidase synthase, NG: naringin, OC: osteocalcin, OPG: osteoprotegerin, BMSC: bone marrow mesenchymal stem cell, ColI: collagen I, ALP: alkaline phosphatase, DMSO: dimethyl sulfoxide, ANOVA: analysis of variance.
$^{*}P<0.05$, $^{**}P<0.01$, $^{***}P<0.001$ vs. DMSO; as evaluated by one-way ANOVA followed by Tukey's test for multiple comparisons. (PTL represented group of 10 μM parthenolide, Bay represented 10 μM Bay 11-7082 (NF-κB inhibitor), NG 10 μM, 1 μM or 0.1 μM represented naringin at 10 μM, 1 μM or 0.1 μM, and rhBMP2 represented 100 ng/mL recombinant human bone morphogenetic protein-2, respectively.

Naringin at 0.1 μM significantly promoted the mRNA expression of OC and OPG in BMSCs at 48 hours ($P<0.01$), while naringin at 0.1 and 1 μM significantly promoted the expression of ColI mRNA in MC3T3-E1 cells at 24 hours (**Figure 2B**). There were no differences in the expression of the remaining mRNAs in these 2 cell lines ($P>0.05$; **Supplementary Figure 2F and G**).

The ALP activity of MC3T3-E1 cells was significantly enhanced by 1 and 10 μM naringin on the third day. Naringin at 0.1 μM significantly promoted ALP activity on day 5, while ALP in the 1 μM naringin group was most active on day 7 ($P<0.05$; **Figure 2D**). The ALP activity of BMSCs non-significantly increased ($P>0.05$; **Supplementary Figure 2C**). Naringin at 0.1 and 1 μM significantly promoted the secretion of OC by BMSCs on days 5 and 7 ($P<0.05$; **Figure 2E**), and the amount secreted on day 7 was higher than that secreted on day 5. The amount of OC secreted by MC3T3-E1 cells did not reach detectable levels.

https://doi.org/10.5051/jpis.2105700285

JPIS
Journal of Periodontal & Implant Science

Treatment of periodontitis in rats with sequentially controlled release by PLLA/CS loaded with parthenolide and naringin

SEM results showed that the periodontitis and periodontal tissue defect model was successfully established (**Supplementary Figure 1C**). Micro-CT showed that after 28 and 56 days of treatment, compared with the model and scaffold groups, the BMD of the periodontal tissue defect area in the DDDS group significantly increased (P<0.01), and the CEJ-ABC distance in the DDDS group significantly decreased after 14, 28, and 56 days of treatment (P<0.05; **Figure 3A and B**). Compared with the model groups, after 28 and 56 days

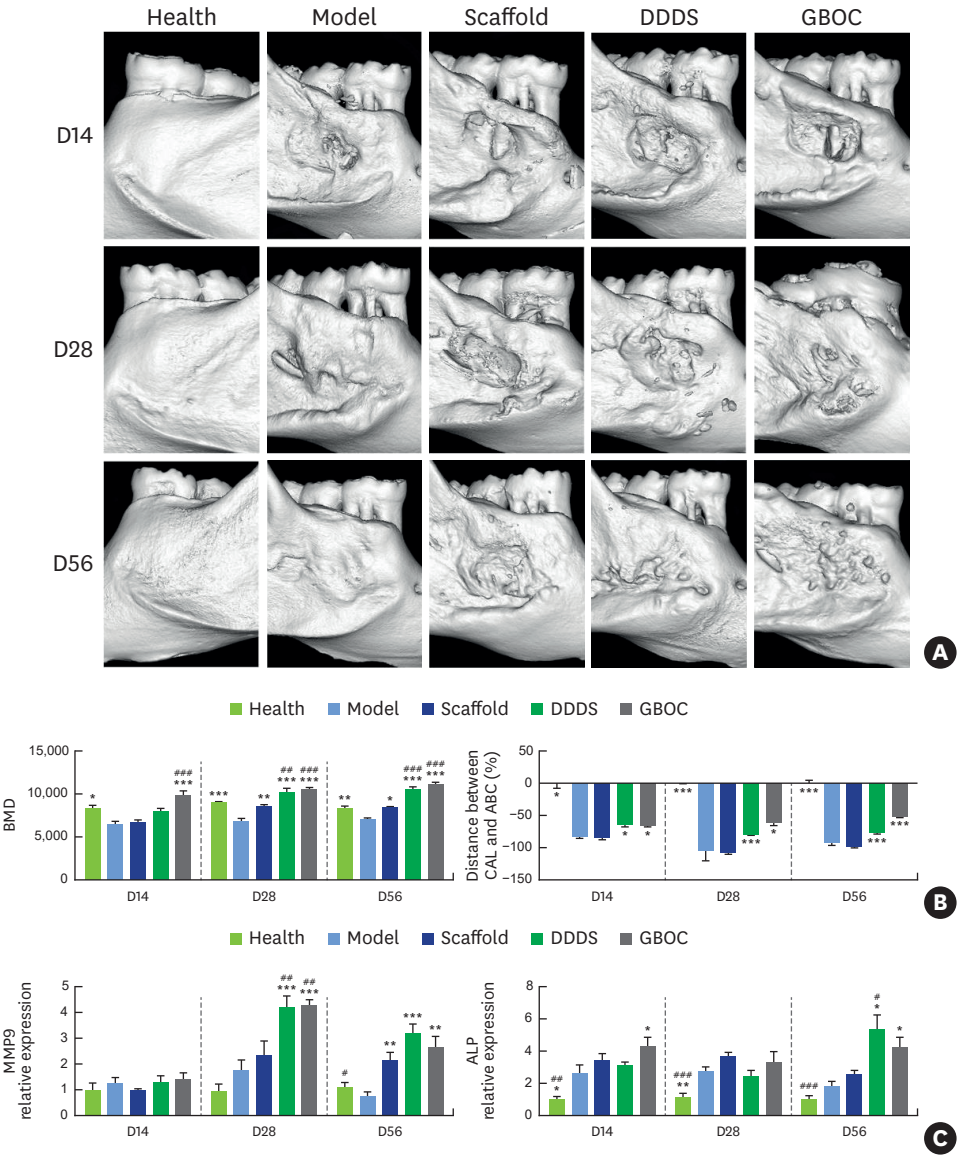

Figure 3. The effects of DDDS loaded with PTL and NG on rat model by micro-CT, and qRT-PCR on different days. (A) Representative samples of surgical defects by micro-CT on different days; (B) the effects of DDDS loaded with PTL and NG on the BMD and the distance between the CEJ-ABC of the surgical defects on different days; (C) the effects of DDDS loaded with PTL and NG on the mRNA expression of MMP9 and ALP on different days.
Values are means ± standard error, D14 (2 week; n=7); D28 (4 weeks; n=9); D56 (8 week; n=10).
CT: computed tomography, DDDS: dual drug delivery scaffold, PTL: parthenolide, NG: naringin, BMD: bone mineral density, CEJ-ABC: cementoenamel junction and alveolar bone crest, MMP: matrix metallopeptidase, ALP: alkaline phosphatase, ANOVA: analysis of variance, PLLA: poly-L-lactic acid, CS: chitosan.
$^{*}P$<0.05, $^{**}P$<001, $^{***}P$<0.001 vs. model; $^{\#}P$<0.05, $^{\#\#}P$<0.01, $^{\#\#\#}P$<0.001 vs. scaffold, as evaluated by one-way ANOVA followed by Tukey's test for multiple comparisons (scaffold represented group that implanted with blank PLLA/CS scaffold, DDDS represented group that implanted with PLLA/CS controlled release system loaded with PTL and NG and GBOC represented group that implanted with Geistlich Bio-OSS® Collagen II respectively).

https://doi.org/10.5051/jpis.2105700285

of treatment, the region of fenestration in the DDDS group had a lower regeneration area, which is consistent with the histomorphometric analysis (**Supplementary Figure 3**).

After 28 and 56 days of treatment, the mRNA expression of *MMP9* in the gingival tissue of the DDDS and GBOC groups was significantly higher than in the model group (P<0.01; **Figure 3C**), while the mRNA expression of *MMP2* in the DDDS group was significantly higher than in the healthy and GBOC groups after 14 days (P<0.05; **Supplementary Figure 2H**). Compared with the scaffold group, the mRNA expression levels of IL-1β and ALP in the DDDS group were significantly higher (P<0.05; **Figure 3C**, **Supplementary Figure 2I**) on day 56.

Compared with the model and scaffold groups, after 14 and 28 days of treatment, the infiltration of inflammatory cells in the DDDS group showed non-significant increasing trends (P>0.05) and then decreased to levels less than those in the healthy group on day 56 (P>0.05; **Figure 4**). After 14 days of treatment, the number of osteoclasts in the DDDS group significantly decreased (P<0.01) compared with the scaffold groups, but significantly increased after 28 days (P<0.001), and significantly decreased after 56 days compared with the scaffold group (P<0.05; **Figure 4**). TNF-α levels significantly decreased in the DDDS group compared with the model and scaffold groups after 56 days, and the ALP levels increased throughout the entire period, with a peak at 28 days (P<0.001; **Figure 5**).

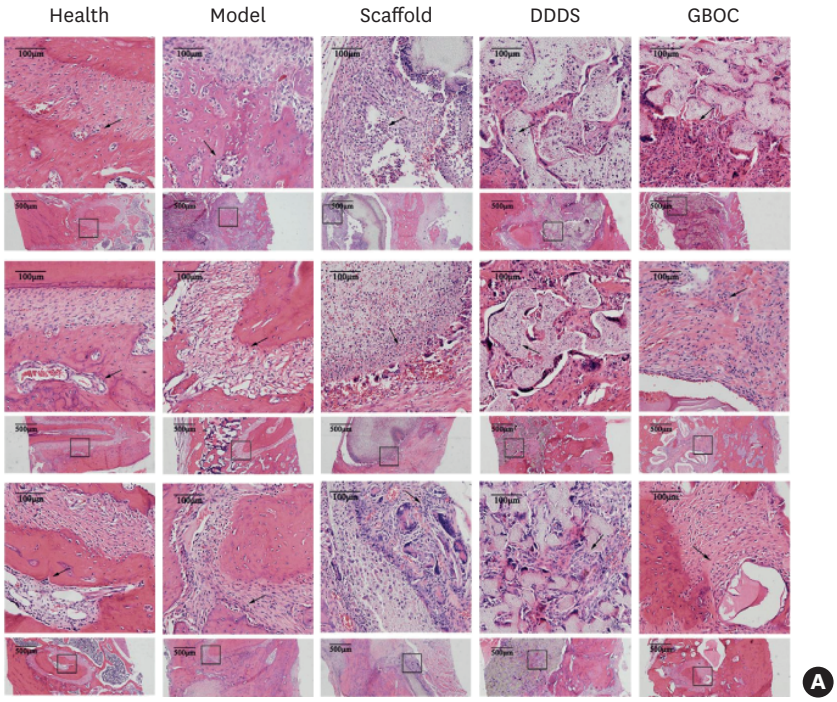

Figure 4. The effects of DDDS loaded with PTL and NG on (A, C) the number of inflammatory cells in the periodontal tissues detected by HE staining, and (B, D) the number of osteoclasts detected by Tartrate-Resistant Acid Phosphatase (TRAP) staining on different days.
Values are means ± standard error (n=3).
DDDS: dual drug delivery scaffold, PTL: parthenolide, NG: naringin, HE: hematoxylin-eosin, TRAP: tartrate-resistant acid phosphatase, ANOVA: analysis of variance, PLLA: poly-L-lactic acid, CS: chitosan.
$^{*}P$<0.05, $^{**}P$<001, $^{***}P$<0.001 vs. model; $^{\#}P$<0.05, $^{\#\#}P$<0.01, $^{\#\#\#}P$<0.001 vs. scaffold as evaluated by one-way ANOVA followed by Tukey's test for multiple comparisons (scaffold represented group that implanted with blank PLLA/CS scaffold, DDDS represented group that implanted with PLLA/CS controlled release system loaded with PTL and NG and GBOC represented group that implanted with Geistlich Bio-OSS® Collagen II respectively).

(continued to the next page)

https://doi.org/10.5051/jpis.2105700285

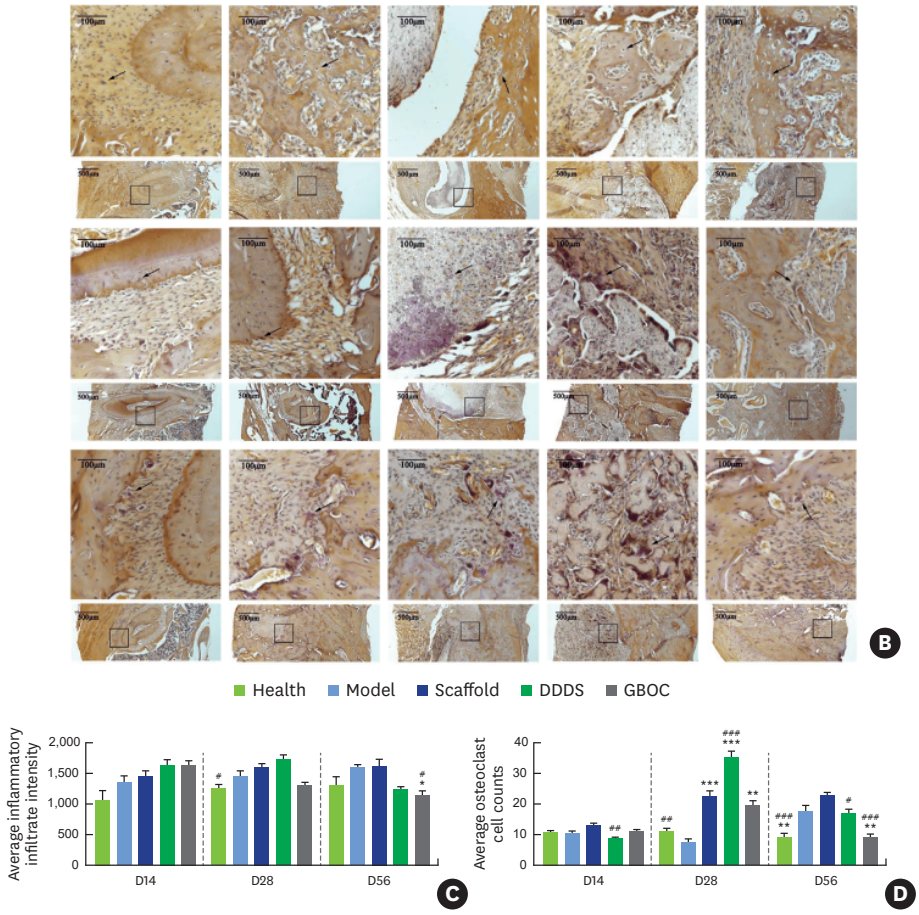

Figure 4. (Continued) The effects of DDDS loaded with PTL and NG on (A, C) the number of inflammatory cells in the periodontal tissues detected by HE staining, and (B, D) the number of osteoclasts detected by Tartrate-Resistant Acid Phosphatase (TRAP) staining on different days.
Values are means ± standard error (n=3).
DDDS: dual drug delivery scaffold, PTL: parthenolide, NG: naringin, HE: hematoxylin-eosin, TRAP: tartrate-resistant acid phosphatase, ANOVA: analysis of variance, PLLA: poly-L-lactic acid, CS: chitosan.
$^{*}P<0.05$, $^{**}P<001$, $^{***}P<0.001$ vs. model; $^{\#}P<0.05$, $^{\#\#}P<0.01$, $^{\#\#\#}P<0.001$ vs. scaffold as evaluated by one-way ANOVA followed by Tukey's test for multiple comparisons (scaffold represented group that implanted with blank PLLA/CS scaffold, DDDS represented group that implanted with PLLA/CS controlled release system loaded with PTL and NG and GBOC represented group that implanted with Geistlich Bio-OSS® Collagen II respectively).

DISCUSSION

Target prediction revealed distinct targets and pathways of parthenolide and naringin (**Figure 1**). HitpickV2, SEA, and SwissTarget predicted that the common target of parthenolide is PTGS2, which plays a specific cyclooxygenase role in the inflammatory response by oxidizing arachidonic acid (AA; C20:4[N-6]) into prostaglandin G2 (PGG2) [20]. Platelet-activating factor receptor (PTAFR) and NOS2 are 2 other common targets of parthenolide, and both have lipopolysaccharide binding receptor activity. PTAFR is involved in various biological processes, such as superoxide formation, cell proliferation, angiogenesis, and inflammatory response regulation [21]. Nitric oxide, the product of NOS2, mediates tumor-killing and bactericidal activities in macrophages [22]. Naringin has 2 common targets. One target is CYP19A1, which catalyzes many reactions involved in the final step of estrogen biosynthesis and drug metabolism and is involved in cell growth and differentiation [23]. Interestingly, the HitpickV2 network also predicted CYP19A1 as a target of parthenolide. The other common naringin target is TAS2R31; however, additional common targets include PTGS1, an analog of PTGS2; Adora3, proline 4-hydroxylase β subunit,

https://doi.org/10.5051/jpis.2105700285

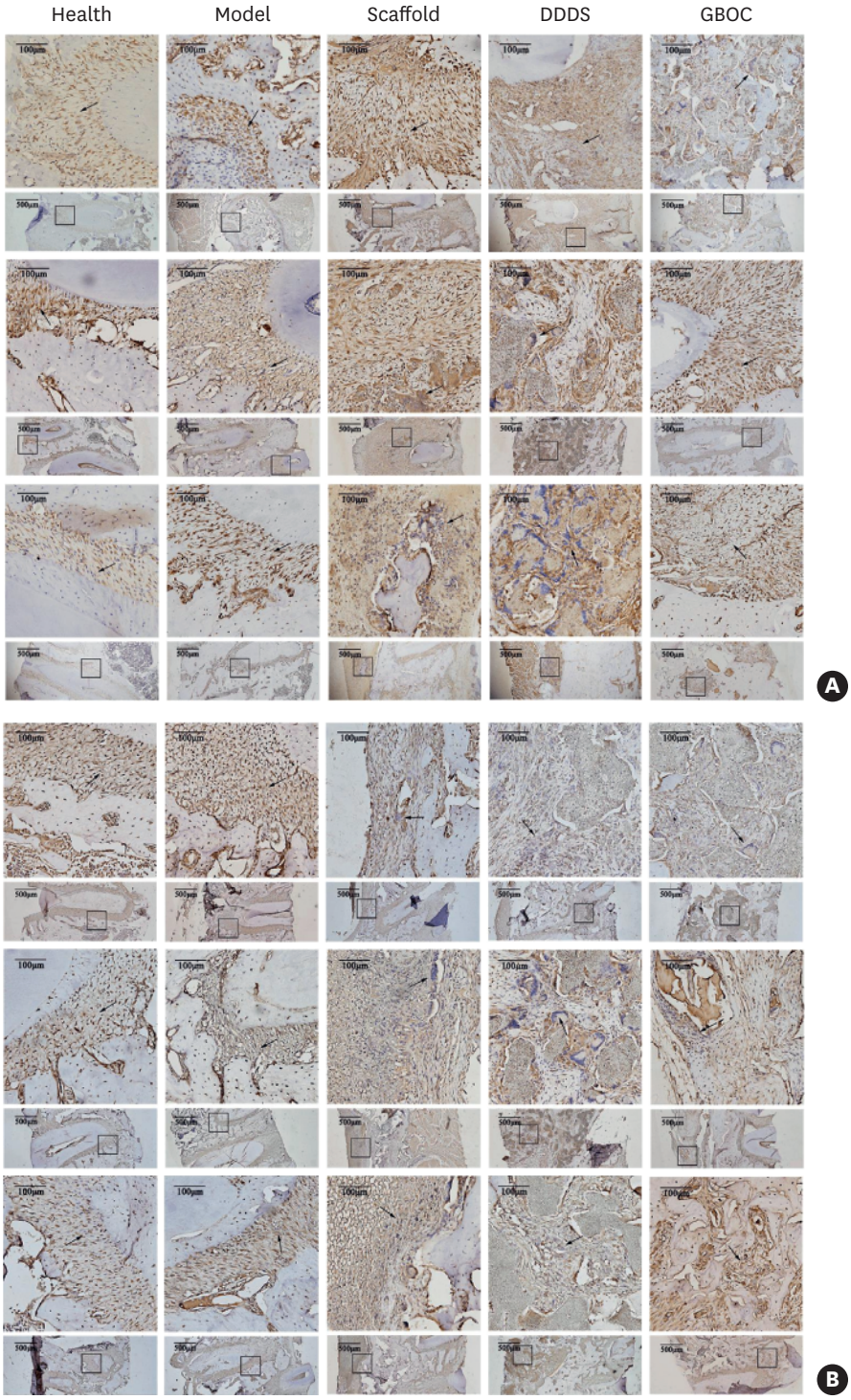

Figure 5. The effects of DDDS loaded with PTL and NG on the expression of (A, C) TNF-α and (B, D) ALP by IHC staining on different days.
Values are means ± standard error (n=3).
DDDS: dual drug delivery scaffold, PTL: parthenolide, NG: naringin, TNF: tumor necrosis factor, ALP: alkaline phosphatase, IHC: immunohistochemical, ANOVA: analysis of variance, PLLA: poly-L-lactic acid, CS: chitosan.
$^{*}P<0.05$, $^{**}P<001$, $^{***}P<0.001$ vs. model; $^{\#}P<0.05$, $^{\#\#}P<0.01$, $^{\#\#\#}P<0.001$ vs. scaffold, as evaluated by one-way ANOVA followed by Tukey's test for multiple comparisons (scaffold represented group that implanted with blank PLLA/CS scaffold, DDDS represented group that implanted with PLLA/CS controlled release system loaded with PTL and NG and GBOC represented group that implanted with Geistlich Bio-OSS® Collagen II respectively).

(continued to the next page)

https://doi.org/10.5051/jpis.2105700285

JPIS
Journal of Periodontal & Implant Science

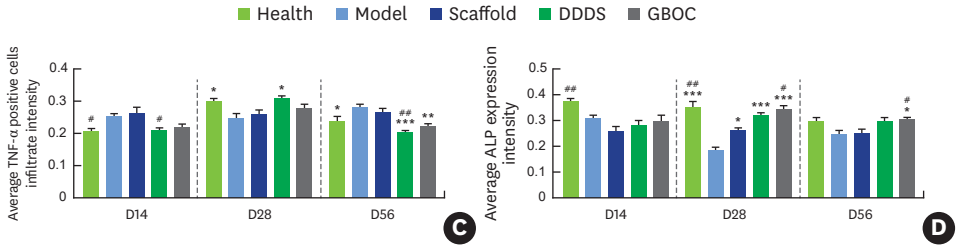

Figure 5. (Continued) The effects of DDDS loaded with PTL and NG on the expression of (A, C) TNF-α and (B, D) ALP by IHC staining on different days.
Values are means ± standard error (n=3).
DDDS: dual drug delivery scaffold, PTL: parthenolide, NG: naringin, TNF: tumor necrosis factor, ALP: alkaline phosphatase, IHC: immunohistochemical, ANOVA: analysis of variance, PLLA: poly-L-lactic acid, CS: chitosan.
$^{*}P<0.05$, $^{**}P<001$, $^{***}P<0.001$ vs. model; $^{\#}P<0.05$, $^{\#\#}P<0.01$, $^{\#\#\#}P<0.001$ vs. scaffold, as evaluated by one-way ANOVA followed by Tukey's test for multiple comparisons (scaffold represented group that implanted with blank PLLA/CS scaffold, DDDS represented group that implanted with PLLA/CS controlled release system loaded with PTL and NG and GBOC represented group that implanted with Geistlich Bio-OSS® Collagen II respectively).

and ubiquitin conjugate E2N [24,25]. In conclusion, the parthenolide-related pathways are mainly involved in fatty acid biosynthesis metabolic processes (such as cyclooxygenase and lipoxygenase) and inflammatory responses, while naringin is primarily involved in the biosynthesis, metabolism, and catabolism of hormones and steroids (particularly sex hormones). The only common pathway of parthenolide and naringin is ovarian steroid production (**Supplementary Table 2**), suggesting that the steroids produced in the body are involved in both the regulation of inflammation and the promotion of new cell synthetic differentiation.

LPS toxicity induces macrophages to secrete numerous cytokines, stimulating the auto cellular immune response and activating the classical NF-κB and mitogen-activated protein kinase (MAPK) pathways [26], thereby damaging the periodontal tissue structure. In this study, parthenolide significantly decreased the mRNA expression of TNF-α, IL-6, IL-1β, IL10, PTGS2, MMP13, and NOS2, the protein expression levels of IL-6 (24 and 48 hours) and TNF-α (24 hours), and the early expression of phospho-p65 and phospho-JNK in RAW264.7 cells stimulated with LPS. We speculated that the mRNA expression of IL-10 in RAW264.7 was inhibited, probably because of the reduced TNF-α expression, as has been reported in the literature [27]. Furthermore, parthenolide has been proven to inhibit the expression of IκB in the NF-κB signaling pathway [28,29]. The present study further confirmed that parthenolide significantly inhibits the expression of phospho-p65 in the IκB downstream signaling pathway and phospho-JNK and phospho-ERK in the MAPK signaling pathway [30]. Therefore, parthenolide exerts a significant combined anti-inflammatory effect on the NF-κB and MAPK signaling pathways. The pharmacological activity of parthenolide on LPS-induced inflammation is stronger than that induced by TNF-α [31], presumably because of its combined inhibitory effect on multiple pathways. The PLLA/PLGA membrane and slowed the release of parthenolide and increased the mRNA expression of all measured cytokines except IL-10 and MMP13 (**Supplementary Figure 2A**), which supports our animal model results.

The OPG/RANKL signaling pathway prevents osteoclast differentiation and maturation, while inhibiting bone resorption [32]. OC is involved in bone mineralization, which is produced exclusively by osteoblasts. ColI is an important component of EMCs, accounting for 80%–90% of all collagen. Low concentrations of naringin significantly promoted the mRNA expression of OC and OPG in BMSCs at 48 hours and the mRNA expression of ColI in MC3T3-E1 cells at 24 hours. Thus, naringin exerts an osteogenic effect, which may vary in different cells. The mechanisms may be that naringin increased the mRNA expression of *OPG* in BMSCs, leading to an increased OPG:RANKL ratio, and then promoted

https://doi.org/10.5051/jpis.2105700285

BMSCs to differentiate into osteogenic cells while directly promoting the maturation and differentiation of MC3T3-E1 cells to express ColI. A study revealed that 2 μg/mL naringin could promote the expression of the RUNX2 and ColI genes on the fourth day and OC on the 8th day in MC3T3-E1 cells pretreated with an ERK1/2 inhibitor [33,34].

ALP is secreted by osteoblasts and is a sign of the early maturation of osteoblasts [35]. Naringin at 1 μM significantly promoted the activity of ALP in MC3T3-E1 cells, while 0.1 μM naringin performed better in BMSCs, and both were most intense on day 7. The secretion of OC protein in BMSCs peaked on day 7; however, in MC3T3-E1 cells, it failed to reach detectable levels.

The DDDS loaded with parthenolide and naringin exerted excellent curative effects in a rat model of periodontitis with periodontal fenestration defects. On day 56, the CEJ-ABC distance in the mandibular first molar of the rats was significantly reduced, and the BMD of the DDDS group significantly increased. The mRNA expression level of MMP9 reached its highest level in the middle stage of treatment, and the relative expression levels of IL-1β and ALP significantly increased at the end of treatment. The results of IHC staining showed that inflammatory cells, osteoclasts, and TNF-α and ALP expression were rare in the health group. In the model group, inflammatory cells accumulated around the bone, and osteoclasts were mostly located in the lacunae at the junction of the bone and periodontal membrane throughout the entire period. In the other 3 groups, many inflammatory cells were found on the edge and inside the scaffold, and many osteoclasts were also observed on the edge of the scaffold. After 28 days, the number of osteoclasts was reduced in the DDDS and GBOC groups. Moreover, the scaffold was gradually degraded and became irregular. The staining color of TNF-α in the DDDS group was darkest in the middle stage of treatment; this result may have been due to the decreased release of parthenolide from the DDDS and the increased degradation of the PLLA scaffolds, which stimulated the production of inflammatory factors to digest these remains. Moreover, ALP expression gradually increased as the chitosan-coated naringin was released and promoted the repair of periodontal tissue defects. Although inflammatory factor expression in the scaffold groups increased, most of these factors accumulated around the scaffold and did not attack the extracellular matrix, and the BMD in the defects increased. These findings indicate the obvious osteogenic effect of the scaffold, and we predict that the increased amount of inflammatory factors possibly promotes the digestion of the scaffold remains rather than aggravating the tissues.

Target predictions and animal experiments both confirmed that parthenolide and naringin have distinct effects. Parthenolide is mainly involved in the inflammatory response, particularly the MAPK pathway. For example, parthenolide significantly inhibits the expression of IL-1β through the predicted common target PTGS2. Naringin promotes osteogenesis by regulating sex hormones, cytochrome P450, and carbonic anhydrase. Our previous study showed that naringenin, the main active metabolite in naringin, acts as a phytoestrogen and has a better osteogenic effect than estrogen (in submission).

In the present system, naringin was creatively encapsulated in CS microspheres and loaded into a PLLA scaffold together with parthenolide to prepare a DDDS, which was implanted into a rat model. Our pilot study confirmed that the system can release parthenolide and naringin in an ordered manner and increase the volume fraction of regenerated bone with excellent biocompatibility [6]. The present study further systematically compared the pharmacological efficacy of this DDDS system. The anti-inflammatory effect was best on day

https://doi.org/10.5051/jpis.2105700285

14, and an obvious osteogenic effect occurred on day 56. Additionally, BMP could promote the differentiation of osteoblasts and induce osteogenesis in MC3T3-E1 and BMSC cells, showing good efficacy in our study. However, the expression and purification of rhBMP2 are challenging, resulting in high costs and limiting its application. The performance of DDDS and GBOC was analogous, and these results indicate promising future applications of DDDS.

Some details warrant further study. For example, DDDS and PLGA/PLLA loaded with parthenolide showed obvious anti-inflammatory effects (**Supplementary Figure 2**), but PLLA/PLGA loaded with naringin did not promote ALP activity in MC3T3-E1 cells (negative results not shown). Nanoparticles loaded with naringin using electrospinning technology prepared by Ji et al. [36] promoted the adhesion, proliferation, differentiation, and mineralization of MC3T3-E1 cells and enhanced ALP secretion, which was not in accordance with our results. Additional evidence of the osteogenic effect of DDDS on periodontal tissue defects in rats is needed. For example, osteoblasts can be detected using Goldner staining, and BMP-2, OPG, OC, and OPN can be detected by IHC staining. Additionally, markers with fluorescent dyes can be added to DDDS to track its metabolic kinetics *in vivo*. Furthermore, the scaffold structure of DDDS loaded with parthenolide and naringin can be optimized to prolong the duration of parthenolide release.

This study systematically proved that DDDS loaded with parthenolide and naringin can treat rats with periodontitis in stages and achieve compound anti-inflammatory and osteogenic effects. This study provides an experimental basis for the clinical use of this DDDS, which has promising prospects for application.

In conclusion, DDDS loaded with parthenolide and naringin displayed ordered anti-inflammatory and osteogenic effects in rats with periodontitis and periodontal tissue defects. The anti-inflammatory effects were strongest at 14 days, while after 56 days, osteogenesis predominated.

SUPPLEMENTARY MATERIALS

Supplementary Table 1

STRING network enrichment (GOBP) of parthenolide and naringin

Click here to view

Supplementary Table 2

STRING network enrichment (KEGG) of parthenolide and naringin

Click here to view

Supplementary Figure 1

Rat periodontitis and fenestration defect model. (A) 2-0 silk thread were ligated around the right mandibular first molars of the rats; (B) picture of periodontal fenestration defects; (C) periodontal fenestration defects by SEM.

Click here to view

https://doi.org/10.5051/jpis.2105700285

Supplementary Figure 2

The effects of drug scaffold *in vivo* and *in vitro*. (A) the effect of PTL + P/P on the mRNA expression of IL-1β, IL-6, TNF-α, MMP13, NOS2 and PTGS2 in RAW264.7 cell; (B) the effect of PTL + P/P and PTL on the mRNA expression of IL-10 in RAW264.7 cell; (C) the effects of NG on the ALP activity of BMSC cell; (D) the effect of PTL + P/P on the protein expressiohosphorospho-p65hosphorospho-ERK in RAW264.7 cI; (E) the effect of PTL + P/P and PTL on the protein expreshosphor phospho-hosphor phospho-ERK in RAW264.7 cell; (F) the effect of NG on the mRNA expression of ALP, OC, OPG and OPN in MC3T3-E1 cells; (G) the effect of NG on the mRNA expression of ALP, OPN, Col 1 and RUNX2 in MC3T3-E1 cells; (H) the effects of DDDS loaded with PTL and NG on the mRNA expression of MMP2 on different days; (I) the effects of DDDS loaded with PTL and NG on the mRNA expression of IL-1β on different days.

Click here to view

Supplementary Figure 3

The effects of DDDS loaded with PTL and NG on the size of periodontal fenestration defects by (A) micro-CT and (B) HE staining on different days.

Click here to view

REFERENCES

1. Straka M, Straka-Trapezanlidis M, Deglovic J, Varga I. Periodontitis and osteoporosis. Neuroendocrinol Lett 2015;36:401-6.
PUBMED
2. Killoy WJ. The clinical significance of local chemotherapies. J Clin Periodontol 2002;29 Suppl 2:22-9.
PUBMED | CROSSREF
3. McAllister BS, Haghighat K. Bone augmentation techniques. J Periodontol 2007;78:377-96.
PUBMED | CROSSREF
4. Cho YD, Seol YJ, Lee YM, Rhyu IC, Ryoo HM, Ku Y. An overview of biomaterials in periodontology and implant dentistry. Adv Mater Sci Eng 2017;2017:1-7.
CROSSREF
5. Ma ZW, Zhang YJ, Wu ZF, Wang R, Zhu H, Li Y, et al. A study on the effect of the chitosan thermosensitive hydrogel loading recombinant human bone morphogenetic protein-2 on repairing periodontal defects. Hua Xi Kou Qiang Yi Xue Za Zhi 2008;26:23-6.
PUBMED
6. Guo Z, Bo D, He P, Li H, Wu G, Li Z, et al. Sequential controlled-released dual-drug loaded scaffold for guided bone regeneration in a rat fenestration defect model. J Mater Chem B Mater Biol Med 2017;5:7701-10.
PUBMED | CROSSREF
7. Wang M, Li Q. Parthenolide could become a promising and stable drug with anti-inflammatory effects. Nat Prod Res 2015;29:1092-101.
PUBMED | CROSSREF
8. Li S, Gao X, Wu X, Wu Z, Cheng L, Zhu L, et al. Parthenolide inhibits LPS-induced inflammatory cytokines through the toll-like receptor 4 signal pathway in THP-1 cells. Acta Biochim Biophys Sin (Shanghai) 2015;47:368-75.
PUBMED | CROSSREF
9. Li N, Jiang Y, Wooley PH, Xu Z, Yang SY. Naringin promotes osteoblast differentiation and effectively reverses ovariectomy-associated osteoporosis. J Orthop Sci 2013;18:478-85.
PUBMED | CROSSREF
10. Pang WY, Wang XL, Mok SK, Lai WP, Chow HK, Leung PC, et al. Naringin improves bone properties in ovariectomized mice and exerts oestrogen-like activities in rat osteoblast-like (UMR-106) cells. Br J Pharmacol 2010;159:1693-703.
PUBMED | CROSSREF

11. Keiser MJ, Roth BL, Armbruster BN, Ernsberger P, Irwin JJ, Shoichet BK. Relating protein pharmacology by ligand chemistry. Nat Biotechnol 2007;25:197-206.
PUBMED | CROSSREF
12. Liu X, Vogt I, Haque T, Campillos M. HitPick: a web server for hit identification and target prediction of chemical screenings. Bioinformatics 2013;29:1910-2.
PUBMED | CROSSREF
13. Daina A, Michielin O, Zoete V. SwissTargetPrediction: updated data and new features for efficient prediction of protein targets of small molecules. Nucleic Acids Res 2019;47:W357-64.
PUBMED | CROSSREF
14. Warde-Farley D, Donaldson SL, Comes O, Zuberi K, Badrawi R, Chao P, et al. The GeneMANIA prediction server: biological network integration for gene prioritization and predicting gene function. Nucleic Acids Res 2010;38:W214-20.
PUBMED | CROSSREF
15. Snel B, Lehmann G, Bork P, Huynen MA. STRING: a web-server to retrieve and display the repeatedly occurring neighbourhood of a gene. Nucleic Acids Res 2000;28:3442-4.
PUBMED | CROSSREF
16. Greene CS, Krishnan A, Wong AK, Ricciotti E, Zelaya RA, Himmelstein DS, et al. Understanding multicellular function and disease with human tissue-specific networks. Nat Genet 2015;47:569-76.
PUBMED | CROSSREF
17. Seol YJ, Pellegrini G, Franco LM, Chang PC, Park CH, Giannobile WV. Preclinical methods for the evaluation of periodontal regeneration in vivo. Methods Mol Biol 2010;666:285-307.
PUBMED | CROSSREF
18. Parsa A, Ibrahim N, Hassan B, van der Stelt P, Wismeijer D. Bone quality evaluation at dental implant site using multislice CT, micro-CT, and cone beam CT. Clin Oral Implants Res 2015;26:e1-7.
PUBMED | CROSSREF
19. Yang X, Zhang H, Wang J, Zhang Z, Li C. Puerarin decreases bone loss and collagen destruction in rats with ligature-induced periodontitis. J Periodontal Res 2015;50:748-57.
PUBMED | CROSSREF
20. Zhou Y, Zhou H, Hua L, Hou C, Jia Q, Chen J, et al. Verification of ferroptosis and pyroptosis and identification of PTGS2 as the hub gene in human coronary artery atherosclerosis. Free Radic Biol Med 2021;171:55-68.
PUBMED | CROSSREF
21. da Silva-Junior IA, Dalmaso B, Herbster S, Lepique AP, Jancar S. Platelet-activating factor receptor ligands protect tumor cells from radiation-induced cell death. Front Oncol 2018;8:10.
PUBMED | CROSSREF
22. Shi FD, Flodström M, Kim SH, Pakala S, Cleary M, Ljunggren HG, et al. Control of the autoimmune response by type 2 nitric oxide synthase. J Immunol 2001;167:3000-6.
PUBMED | CROSSREF
23. Di Nardo G, Zhang C, Marcelli AG, Gilardi G. Molecular and structural evolution of cytochrome P450 aromatase. Int J Mol Sci 2021;22:631.
PUBMED | CROSSREF
24. Zhang J, Guo S, Wu Y, Zheng ZC, Wang Y, Zhao Y. P4HB, a novel hypoxia target gene related to gastric cancer invasion and metastasis. BioMed Res Int 2019;2019:9749751.
PUBMED | CROSSREF
25. Yin P, Tu Z, Yin A, Zhao T, Yan S, Guo X, et al. Aged monkey brains reveal the role of ubiquitin-conjugating enzyme UBE2N in the synaptosomal accumulation of mutant huntingtin. Hum Mol Genet 2015;24:1350-62.
PUBMED | CROSSREF
26. Li Q, Valerio MS, Kirkwood KL. MAPK usage in periodontal disease progression. J Signal Transduct 2012;2012:308943.
PUBMED | CROSSREF
27. Smallie T, Ross EA, Ammit AJ, Cunliffe HE, Tang T, Rosner DR, et al. Dual-specificity phosphatase 1 and tristetraprolin cooperate to regulate macrophage responses to lipopolysaccharide. J Immunol 2015;195:277-88.
PUBMED | CROSSREF
28. Kwok BH, Koh B, Ndubuisi MI, Elofsson M, Crews CM. The anti-inflammatory natural product parthenolide from the medicinal herb Feverfew directly binds to and inhibits IkappaB kinase. Chem Biol 2001;8:759-66.
PUBMED | CROSSREF

29. Wang D, Wang H, Fu S, Cheng X, Yang F, Zhang Q, et al. Parthenolide ameliorates Concanavalin A-induced acute hepatitis in mice and modulates the macrophages to an anti-inflammatory state. Int Immunopharmacol 2016;38:132-8.
PUBMED | CROSSREF

30. Feng D, Ling WH, Duan RD. Lycopene suppresses LPS-induced NO and IL-6 production by inhibiting the activation of ERK, p38MAPK, and NF-kappaB in macrophages. Inflamm Res 2010;59:115-21.
PUBMED | CROSSREF

31. de Oliveira RR, Schwartz-Filho HO, Novaes AB Jr, Taba M Jr. Antimicrobial photodynamic therapy in the non-surgical treatment of aggressive periodontitis: a preliminary randomized controlled clinical study. J Periodontol 2007;78:965-73.
PUBMED | CROSSREF

32. Carda C, Silvestrini G, Gomez de Ferraris ME, Peydró A, Bonucci E. Osteoprotegerin (OPG) and RANKL expression and distribution in developing human craniomandibular joint. Tissue Cell 2005;37:247-55.
PUBMED | CROSSREF

33. Chen LL, Lei LH, Ding PH, Tang Q, Wu YM. Osteogenic effect of *Drynariae rhizoma* extracts and *Naringin* on MC3T3-E1 cells and an induced rat alveolar bone resorption model. Arch Oral Biol 2011;56:1655-62.
PUBMED | CROSSREF

34. Yin L, Cheng W, Qin Z, Yu H, Yu Z, Zhong M, et al. Effects of naringin on proliferation and osteogenic differentiation of human periodontal ligament stem cells *in vitro* and *in vivo*. Stem Cells Int 2015;2015:758706.
PUBMED | CROSSREF

35. Jo S, Han J, Lee YL, Yoon S, Lee J, Wang SE, et al. Regulation of osteoblasts by alkaline phosphatase in ankylosing spondylitis. Int J Rheum Dis 2019;22:252-61.
PUBMED | CROSSREF

36. Ji Y, Wang L, Watts DC, Qiu H, You T, Deng F, et al. Controlled-release naringin nanoscaffold for osteoporotic bone healing. Dent Mater 2014;30:1263-73.
PUBMED | CROSSREF

https://doi.org/10.5051/jpis.2105700285